The role and analysis of molecular systems in electrocatalysis

Dijk, B. van

Appendix C

Supplementary information for Chapter 4:
A selective molecular dinuclear copper oxygen reduction catalyst for the electrochemical synthesis of H_2O_2 at neutral pH

C.1 UV-vis of Cu_2(btmpa) and H_2O_2

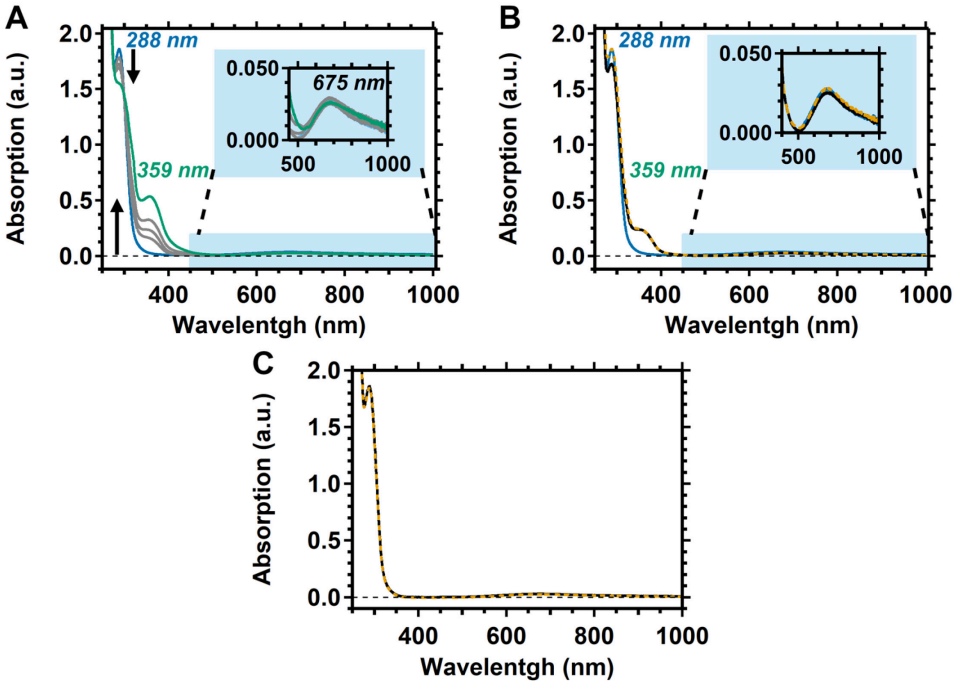

Figure C.1. UV-Vis of 0.15 mM **Cu_2(btmpa)** in phosphate buffer. A fresh solution (blue trace) spiked with 1.13 mM H_2O_2 was monitored over the course of a week (green trace) (A). B shows a fresh and 8 hour old solution (blue and black trace, respectively) with H_2O_2 and an 8 hour old **Cu_2(btmpa)** solution after performing O_2 reduction at 0.0 V (orange dashed). A fresh (black) and 1 week old solution of **Cu_2(btmpa)** (orange dashed) without H_2O_2 is shown in C.

C.2 EPR and SQUID of Cu_2(btmpa)

The electron paramagnetic resonance (EPR) spectra of **Cu_2(btmpa)** were measured in water, 0.1 M phosphate buffer and dimethyl formamide (Figure C.2). In water and phosphate buffer, broad peaks were observed and two g values could be extracted from the simulation: $g_{||}$ = 2.21 and $g_{\perp}$ = 2.08 for water and $g_{||}$ = 2.23, $g_{\perp}$ = 2.06 for phosphate buffer though the latter simulation was less accurate. The spectra and g values are very similar but minor discrepancies suggest that phosphate coordination slightly changes the geometry around the copper cores though pH effects are not excluded. In dimethyl formamide, a clear splitting pattern arising from coupling to the copper core was observed. The g values of dimethyl formamide are $g_{||}$ = 2.23 (A_{Cu} = 500 Hz) and $g_{\perp}$ = 2.06, equal to the phosphate buffer sample.

This might indicate that both dimethyl formamide and phosphate have a similar influence on the geometry. Because $g_{||} > g_{\perp}$, the single occupied molecular orbital (SOMO) is the $d_{x^2-y^2}$ orbital since there is significant orbital mixing in the *z*-direction ($g_{||} = g_z$). This is the case in, for example, an elongated (distorted octahedron).[1] Hence, the geometry of **Cu_2(btmpa)** in aqueous and dimethyl formamide solutions is in close resemblance to the previously published crystal structures.[2] The obtained g tensors are clearly different from the mononuclear **Cu(tmpa)** complex ($g_{||} = 2.00$, $g_{\perp} = 2.19$) indicating a significant difference in geometry.[3] In the case of **Cu(tmpa)**, $g_{||} < g_{\perp}$, pointing to d_{z^2} as SOMO and a trigonal bipyramidal geometry of the complex.[1] Overall, it seems that both copper centra of **Cu_2(btmpa)** can be seen as independent and produce the same EPR signal. There is no antiferromagnetic coupling as was also observed with SQUID (superconducting quantum interference device, Figure C.3). Interestingly, the g value for both copper centra was found to be 1.85 from the powder SQUID spectra which indicates that they are identical but have a lower value than determined from the frozen solution EPR spectra. It has to be noted that g values from EPR are

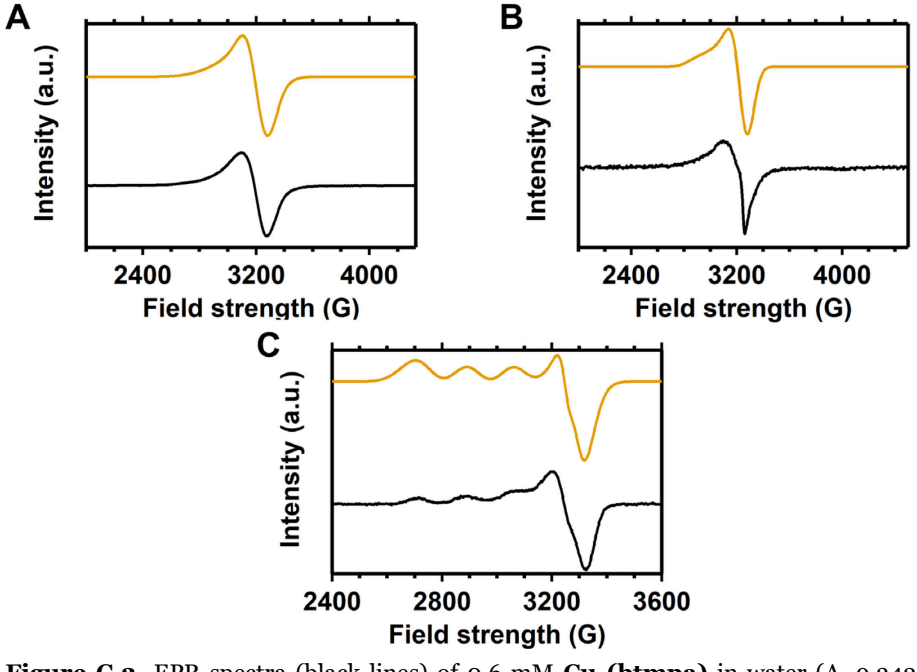

Figure C.2. EPR spectra (black lines) of 0.6 mM **Cu_2(btmpa)** in water (A, 9.342 GHz), phosphate buffer (B, 9.344 GHz) and dimethyl formamide (C, 9.352 GHz). The simulated spectra are shown in orange. Spectra were obtained at 77 K with frozen solutions.

generally more accurate than g values obtained from fitted SQUID data. From the SQUID data it can also be concluded that there is a small ferromagnetic coupling between the two copper centra of 34 cm^{-1}. From the data, no conclusive evidence for the coordination of the copper centra with respect to each other can be given. On the other hand, the coupling does indicate that the two copper centra have a minor influence on each other.

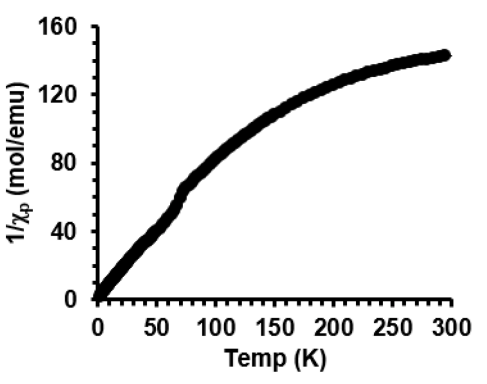

Figure C.3. SQUID spectrum of **Cu_2(btmpa)** powder.

C.3 The collection efficiency of H_2O_2 of Pt

For reliable rotating ring disk electrode (RRDE) measurements, the collection efficiency has to be stable throughout the measurement. That way, the percentage of H_2O_2 and the electron transfer number (n) can be determined using equations C.1 and C.2 respectively where $N_{H_2O_2}$ is the collection efficiency for H_2O_2. Usually, this collection efficiency can be determined with a one-electron redox couple such as the $[Fe^{II}CN_6]^{4-}/[Fe^{III}CN_6]^{3-}$ and equation C.3 where N_{CE} is the collection efficiency. However, H_2O_2 oxidation on Pt is not always diffusion limited. As a result, the H_2O_2 collection efficiency ($N_{H_2O_2}$) can be different from the N_{CE} determined with the $Fe^{II/III}$ redox couple.[4] Phosphate buffer and PtO_x formation at 1.2 V can significantly influence the amount of active sites thereby changing the potential where diffusion limited H_2O_2 oxidation is obtained on a Pt ring.[5-11] To study what factors influence $N_{H_2O_2}$, several chronoamperometry measurements were performed with the RRDE setup using a GC disk as work electrode in O_2 purged 0.1 M phosphate buffer of pH 7. The GC electrode is a 100% selective catalyst at moderate potentials in the freshly polished state.[12]

$$\%H_2O_2 = \frac{2 \times (\frac{i_{ring}}{N_{H_2O_2}})}{i_{disk} + (\frac{i_{ring}}{N_{H_2O_2}})} \times 100\% \qquad \textbf{Eqn. C.1}$$

$$n = \frac{4 \times i_{disk}}{i_{disk} + (\frac{i_{ring}}{N_{H_2O_2}})} \qquad \textbf{Eqn. C.2}$$

$$N_{CE} = \frac{|i_{ring}|}{|i_{disk}|} \qquad \textbf{Eqn. C.3}$$

To start, we studied the influence of the disk potential (Figure C.4). The ring and disk currents were stable at disk potentials (0.1, 0.0, and −0.1 V) where low current is obtained (Figure C.4A). The corresponding collection efficiencies are lower than the theoretical value of 24% for this specific setup (Figure C.4B). The maximum collection efficiency can be achieved by not only mechanically polishing the Pt ring, but also electropolishing the ring to remove any poisoning substances from the Pt

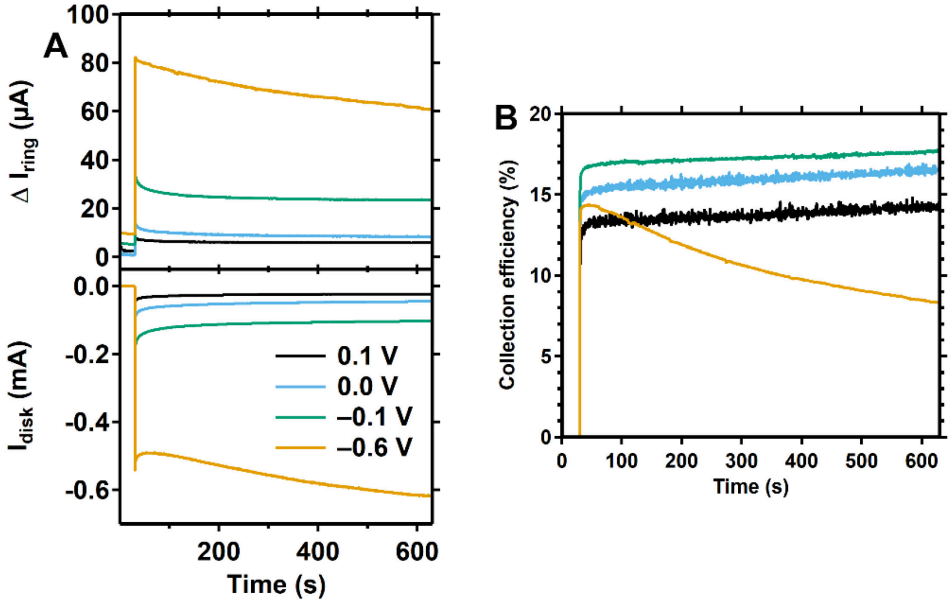

Figure C.4. RRDE Chronoamperometry of O_2 reduction by a GC disk at various potentials (A, bottom panel), the response of the Pt ring (A, top panel), and the calculated collection efficiency of the ring for H_2O_2 (B). The ring was kept at 1.2 V. The disk was rotated at 1600 rpm. All electrodes were polished before the measurement. O_2 purged 0.1 M phosphate buffer of pH 7 was used.

surface. However, we found that such a clean Pt surface is very susceptible for (re-)poisoning and therefore the collection efficiency will drop quickly over the course of the experiment. When merely mechanical polish is applied, the collection efficiency shows a minor incline over the course of the 10 minute experiment (Figure C.4B) and is therefore more useful. Nevertheless, only a low amount of H_2O_2 is produced at these potentials since the disk current is low. The disk produces up to 6 times more current at −0.6 V. Interestingly, the disk current increases over the course of 10 minutes whereas the ring current decreases at that potential. As the ratio ring to disk current decreases rapidly, the calculated collection efficiency (Figure C.4B) decreases from 14 to 8% over the course of 10 minutes at −0.6 V disk potential. Two explanations are possible. First, the selectivity of O_2 to H_2O_2 might not be 100% at this potential but instead an increasing part of the current might be attributed to the over-reduction of H_2O_2 to H_2O. The second explanation is that the Pt ring surface is affected by H_2O_2 and therefore less able to oxidize H_2O_2.

To study whether the Pt surface is affected by H_2O_2, we performed two RRDE amperometry measurements at 0.0 V for 10 minutes. First, a freshly polished GC and Pt ring were used (Figure C.5). After the first 0.0 V measurement, amperometry at −0.6 V was performed for 10 minutes in order to expose the Pt ring to a large amount of H_2O_2. Finally, another 0.0 V amperogram was recorded for 10 minutes. The disk current at 0.0 V for the last measurement is lower than it the freshly polished state, but more stable at −45 μA. The current of the freshly polished GC decreases to circa −50 μA after 10 minutes. On the other hand, the ring current has significantly dropped from circa 10 μA to 5 μA in the 0.0 V measurement after the −0.6 V measurement. Moreover, the ring to disk ratio, and consequently the calculated collection efficiency, drops significantly over the 10 minute experiment from 15 to 9%. In conclusion, the Pt ring is somehow affected and cannot consistently oxidize H_2O_2 after being exposed to larger amounts of H_2O_2. Indeed, earlier reports have shown that H_2O_2 inhibits H_2O_2 oxidation by Pt at high (>1 mM) H_2O_2 concentration as the process is a mix of diffusion and kinetical parameters.[13] Therefore, the application of RRDE for the detection of H_2O_2 remains limited to situations where a low amount of H_2O_2 is produced and/or a qualitative one where only the detection is important. Quantification of H_2O_2 in situations with larger amounts of H_2O_2 is limited under these conditions.

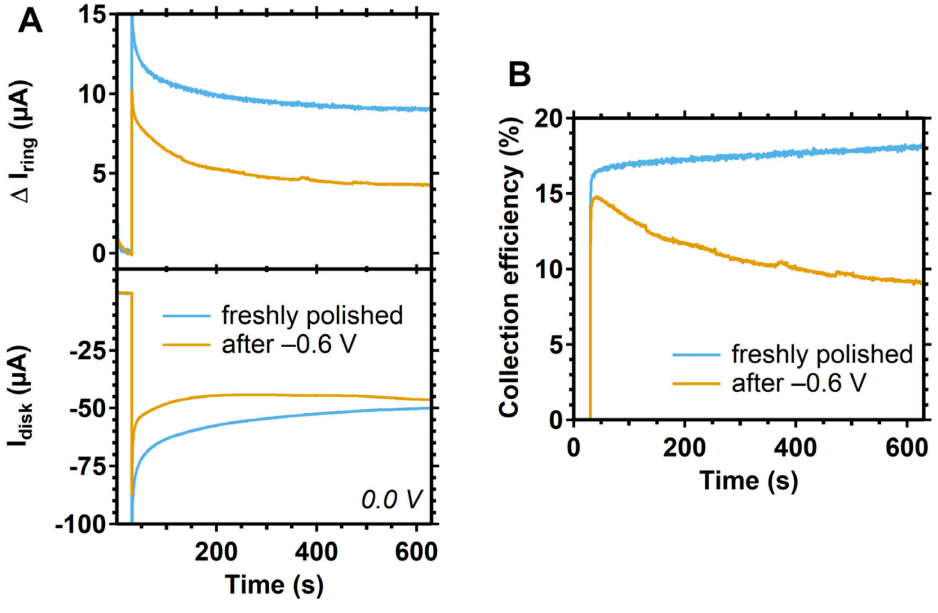

Figure C.5. RRDE chronoamperometry of O_2 reduction at 0.0 V for 10 minutes (A, bottom panel), the Pt ring response (A, top panel) with a freshly polished GC an Pt ring (blue) and after an experiment that produced high amounts of H_2O_2 (orange). The corresponding calculated collection efficiencies (or ring to disk ratios) are shown in B. Prior to the yellow measurement, an amperogram at –0.6 V was recorded for 10 minutes. The ring was kept at 1.2 V. The same conditions as in Figure C.4 were used.

C.4 Electrochemical H_2O_2 reduction by Cu_2(btmpa)

Over-reduction of H_2O_2 to H_2O is a possibility that could lower the H_2O_2 selectivity. Therefore, H_2O_2 reduction by **Cu_2(btmpa)** under argon atmosphere was studied by CV (Figure C.6). The reduction of different concentrations of H_2O_2 was studied under rotating and non-rotating conditions. Indeed, there is reducing current observed indicating that H_2O_2 is reduced by the complex. A positive order in H_2O_2 is expected for the rate determining step because the reducing current increases with the H_2O_2 concentration. Interestingly, no peak current under non-rotating and no diffusion limited current under rotating conditions could be obtained even at high concentrations of H_2O_2. Only at 1.2 mM, a peak current and limiting current seem to be reached. However, these disk currents of 50 μA are low and not close to 200 μA which is the diffusion limited current for H_2O_2 reduction under these conditions.[4] Overall, the reduction of H_2O_2 by **Cu_2(btmpa)** is a slow, kinetically limited reaction. Therefore, O_2 reduction to H_2O_2 by **Cu_2(btmpa)** can

reach a high selectivity in this potential window. However, this selectivity may decrease significantly when the concentration of H_2O_2 rises during long experiments.

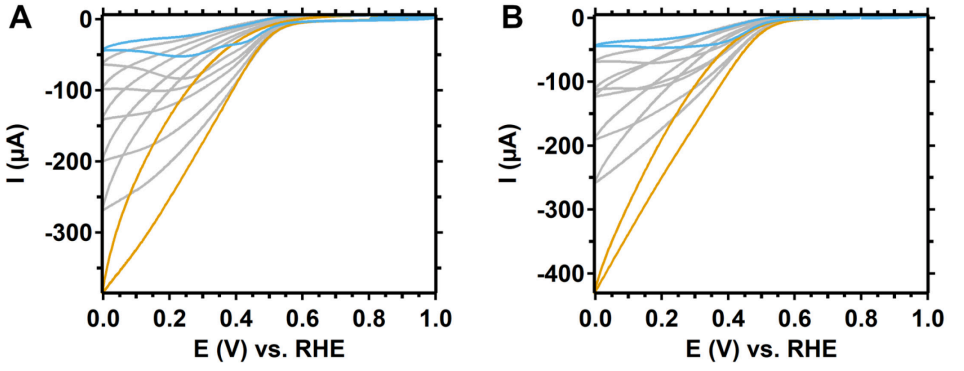

Figure C.6. Cyclic voltammograms of H_2O_2 reduction by 0.15 mM **Cu_2(btmpa)** under argon atmosphere with a non-rotating (A) and rotating (B, 1600 rpm) GC electrode (0.196 cm^2). H_2O_2 concentrations of 1.2 (blue), 2.1, 4.2, 8.4, 14.1, 25.2, and 47.4 mM (orange) were tested in 0.1 M phosphate buffer of pH 7. Scan rates of 100 mV/s (A) and 50 mV/s (B) were used.

C.5 Cu^0 deposit on electrode

After 7 hours of continuously applying 0.0 V in a **Cu_2(btmpa)** solution, a clear copper-colored deposit will form (Figure C.8). Frequent intervals at 0.8 V might help to strip this deposit. However, there is an additional process already from the start of the measurement: during the first half hour of amperometry at 0.0 V a significant increase in current is observed. Moreover, in the first 2 hours of amperometry with 0.8 V intervals, the magnitude of the current at the end of each cycle is regained at the start of the next cycle after the interval (Figure 4.5). Apparently, the deposit causing this increase in current cannot be simply removed by applying 0.8 V. On the other hand. an electrode that was held in a **Cu_2(btmpa)** solution only for the first half hour and subsequently rinsed with water did not retain its activity. When this electrode was put in catalyst-free electrolyte after rinsing to compare the activity with a polished GC electrode, the current drops significantly to −0.08 mA and is equal the current of the polished GC (Figure C.7). This in in contrast to what happens when the electrode stays in catalyst solution (Figure 4.5). In that case, the current remains −0.37 mA even after briefly applying a potential of 0.8 V. The rinsing of the electrode is the extra step that removed most of the deposit on the electrode. When the rinsed electrode was tested for an additional 5 hours, the current steadily increased to −0.27 mA. It did not reach the level of an electrode that permanently resides in a **Cu_2(btmpa)** solution (−0.83 mA) but it did follow a

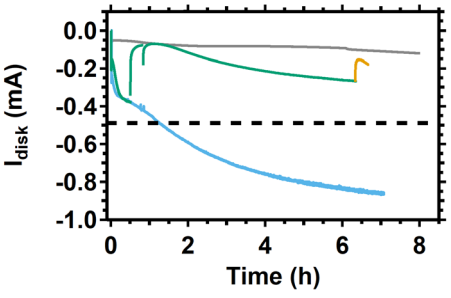

Figure C.7. Rotating (1600 rpm) disk electrode experiment at 0.0 V of a glassy carbon electrode in O_2 saturated electrolyte in absence (grey) or in presence (blue) of **Cu_2(btmpa)**. The green trace was in presence of **Cu_2(btmpa)** for 30 minutes after which the electrode was rinsed and tested in a catalyst-free electrolyte. The orange trace is a 20 minute measurement recorded after the electrode (green trace) was briefly held at 0.8 V. 0.1 M phosphate buffer of pH 7 was used. Catalyst concentration was 0.15 mM.

similar current profile. Also, the polished GC does not show this behavior (Figure C.7). These results seem to point to a small residue of **Cu_2(btmpa)** still residing on the electrode even after the rinse. Although the EQCM data show that the potential-dependent adsorption is reversible on gold electrodes, the carbon based GC electrode might have a stronger affinity with **Cu_2(btmpa)**. Especially in the first half hour of amperometry, catalyst accumulation on the electrode enhances the number of active sites. At 0 V, **Cu_2(btmpa)** is still significantly kinetically limited. In this case, an increase in active sites would indeed increase the catalytic current. The 0.8 V intervals do not lead to significant desorption of **Cu_2(btmpa)** perhaps aided by the continuous supply of fresh catalyst by the rotation of the electrode. Rinsing with water on the other hand, did remove most catalyst. The small residue that would still be present was then subjected to 0.0 V for 5 hours. In that time window, this residue can form Cu^0 which explains why the current steadily

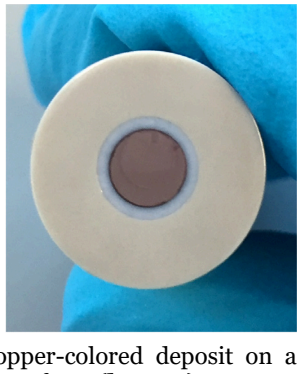

Figure C.8. Picture of the copper-colored deposit on a GC electrode after 7 hours of amperometry at 0.0 V in presence of **Cu_2(btmpa)**.

increases more than that of a polished GC (Figure C.7). Indeed, after applying a short 0.8 V interval, the current significantly decreased to −0.15 mA which indicated the stripping of Cu^0 (Figure C.7).

C.6 Intercepting H_2O_2 during long term chronoamperometry

To study long term H_2O_2 production with a rotating ring disk electrode setup, we performed amperometry at 0.0 V in 20 minute intervals for a period of 8.5 hours. In the 10 second intervals, potentials of 0.55 V applied at the Pt ring to reduce accumulated PtO_x and 0.8 V at the disk to strip Cu^0 were applied. Additionally, a 30 second baseline measurement was included in the interval procedure after 3 hours by holding the 0.8 V potential at the disk while setting the ring to 1.2 V. Consequently, no H_2O_2 is produced at the disk and only H_2O_2 that is already present in the solution is detected at the Pt ring. The results of this measurement are shown in Figure C.9 including the schematic overview of the measurement procedure. With the additional ring data, it is clear that H_2O_2 is formed at the disk. When the

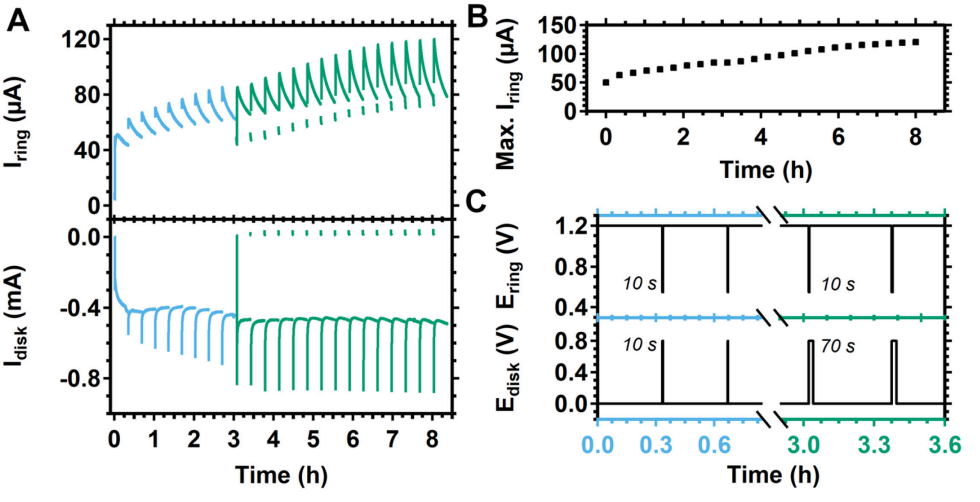

Figure C.9. RRDE chronoamperometry measurement of O_2 reduction at 0.0 V by **Cu_2(btmpa)** over the course of 8.5 hours with an interval every 20 minutes (A) with the disk (bottom) and ring current (top). The maximum ring current reached every 20 minutes is depicted in B and the potential *versus* time plot in C for the blue and green marked areas of A. During the short interval (10 seconds), accumulated PtO_x on the ring could be reduced and Cu^0 on the disk could be stripped by a potential of 0.55 V and 0.8 V, respectively. After 3 hours, the disk potential was kept at 0.8 while the ring was set to 1.2 V for 1 minute to establish a baseline ring current.

measurement starts, the ring current immediately rises to 50 μA which (with a pre-determined N_{CE} of 18.3% for this measurement) corresponds to a 91% selectivity for H_2O_2. However, the ring current decreases to 45 μA and the selectivity drops to 72% over the course of 20 minutes. Every 20 minute cycle, the maximum of the ring current was reached in the first minute of the measurement after which the current decreased. As discussed before, the ring current can also decrease because of PtO_x formation and/or exposure to high amounts of H_2O_2. Indeed, the ring current increased to 65 μA after the first interval wherein the potential of the ring was briefly set to 0.55 V demonstrating that the decrease in ring current is mostly caused by these events and not (entirely) by a decrease in selectivity of H_2O_2 production. This was found to be the case for every 20 minute measurement. From that, we conclude that H_2O_2 is produced throughout the measurement with a high selectivity. Remarkably, 100% H_2O_2 production should only lead to a maximum current of 60 μA at the ring. Already in the second 20 minute cycle the maximum ring current is 65 μA. This indicates that H_2O_2 from the solution is oxidized as well. The maximum ring current increased every 20 minute cycle (Figure C.9B) which is expected if H_2O_2 is accumulating in the solution. Hence, a baseline measurement was added to the interval procedure after 3 hours to establish the ring current before H_2O_2 is produced at the disk. The baseline current after 3 hours was 50 μA and increased over time to circa 80 μA showing that H_2O_2 is accumulating in the solution. Interestingly, the disk current hardly increases and remains stable after 3 hours. Moreover, the increase during each 20 minute cycle is not less pronounced as was found in measurements without the Pt ring electrode (Figures 4.5 and C.10). Most likely, the continuous re-oxidation of a part of the formed H_2O_2 and the H_2O_2 from the solution will limit the concentration of H_2O_2 in the solution. In turn, this would indicate that high H_2O_2 concentrations would lead to faster Cu^0 deposition and more over-reduction of H_2O_2 thereby increasing the current rapidly during each 20 minute cycle.

C.7 The influence of interval measurements on the Faradaic efficiency

As described, Cu^0 deposition can become a problem and negatively affect the Faradaic efficiency. Two experiments were performed to check whether an interval measurement would increase the Faradaic efficiency by briefly applying a potential of 0.8 V every 20 minutes. The results are plotted in Figure C.10. Notably, the Faradaic efficiency decreases over time in both the continuous as well as the interval

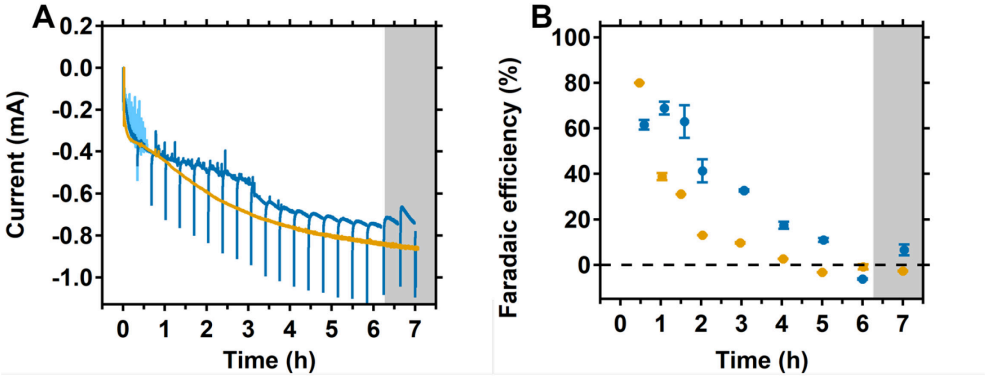

Figure C.10. Rotating disk measurement at 0.0 V of O_2 reduction by **Cu_2(btmpa)** over the course of 7 hours (A) and the corresponding Faradaic efficiency (B). Each datapoint is the efficiency of the period since the preceding datapoint. A continuous measurement (orange) and an interval measurement (blue) were monitored. A potential of 0.8 V was briefly applied during the intervals. The spikes are an artefact of (re-)applying 0.0 V. In the grey area, the 0.8 V interval time was extended to 4 minutes. The same conditions as Figure 4.5 were used.

measurement. The efficiency of the continuous measurement is lower than the interval measurement, apart from the first 30 minutes. In these first 30 minutes, the Faradaic efficiency for H_2O_2 is high: 80% for the continuous and 62% for the interval-experiment. The lower Faradaic efficiency for the interval experiment could be explained from the high current noise in these 30 minutes. The measurement

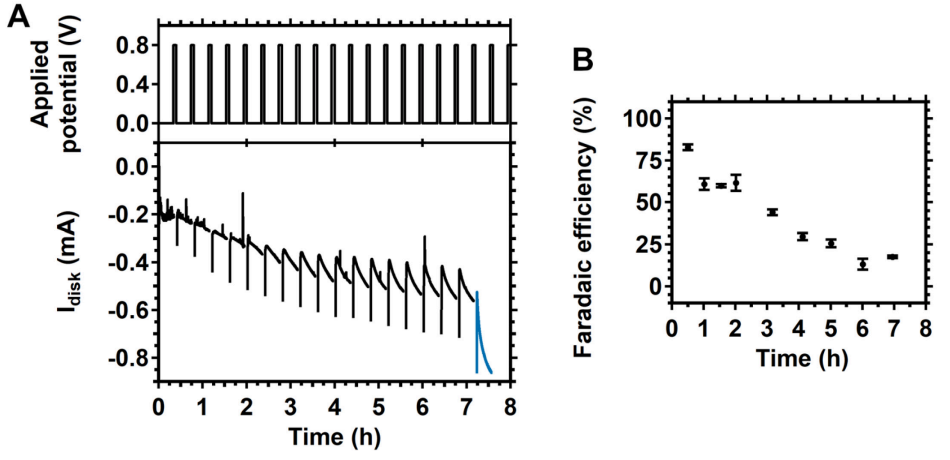

Figure C.11. Rotating disk measurement at 0.0 V of O_2 reduction by **Cu_2(btmpa)** (A) and the corresponding Faradaic efficiency (B). The full 8 hours of the measurement of Figure 4.6 is depicted. Before the last 20 minutes (blue line in A), the H_2O_2 concentration was manually increased 5 times.

suffered from O_2 bubbles blocking the surface during continuous purging which resulted in current spikes and a higher overall charge that passed the electrode. After 30 minutes, the set-up of the disk electrode was slightly changed to overcome this problem. As a result, the Faradaic efficiency increased to 69% in the next 30 minutes. This in sharp contrast to the continuous experiment. There, the efficiency dropped to 39%. 1.5 hours after the start, it dropped even further to 31% while the interval measurement still had an efficiency of 63%. Clearly, the 0.8 V interval could strip away Cu^0 thereby keeping the Faradaic efficiency high. This is also reflected in the disk current which was lower for the interval experiment than for the continuous experiment. The latter used more charge for the full 4 electron reduction to water. Nonetheless, the Faradaic efficiency dropped significantly for the interval experiment as well after 2 hours. After 6 hours, the calculated efficiency was negative because there had been a decrease in the H_2O_2 bulk concentration. This happened for the continuous measurement already after 5 hours. When the calculated selectivity is negative, more H_2O_2 is converted to H_2O than that H_2O_2 is produced from O_2. For the continuous experiment this was expected because of the slow build-up of Cu^0, but not for the interval experiment. The 30 second 0.8 V interval was apparently not enough to strip all the formed Cu^0. Therefore, the interval time was increased to 4 minutes after 6 hours of amperometry (marked by the grey area in Figure C.10). As a result, the Faradaic efficiency went back to a positive value of 6%

Table C.1. The concentration of H_2O_2 as measured by the enzyme based photometric method for Figure C.11. The volume of the solution changed continuously during the measurement as aliquots were taken. Errors are as standard errors.

Hours after start	Faradaic efficiency[a] (%)	Concentration H_2O_2 (mM)	Volume of electrolyte (ml)
00:30	83 ± 2 (3)	0.040 ± 0.001	33.6
01:01	61 ± 3 (3)	0.077 ± 0.003	32.0
01:33	60 ± 1 (3)	0.124 ± 0.001	30.7
02:01	62 ± 5 (3)	0.166 ± 0.006	29.2
03:10	44 ± 2 (3)	0.273 ± 0.007	27.6
04:07	30 ± 2 (4)	0.340 ± 0.009	26.2
05:01	26 ± 3 (4)	0.41 ± 0.01	24.9
06:01	13 ± 3 (5)	0.45 ± 0.02	23.4
06:57	18 ± 1 (3)	0.503 ±0.005	21.9

[a]The Faradaic efficiency corresponds to the period between measurements, not the total Faradaic efficiency since the start of the measurement. Number between brackets is the amount of measurements that was performed.

and the disk current decreased. The bulk H_2O_2 concentration went up from 15.6 to 16.7 mg/l which is 0.5 mM of H_2O_2. Overall, these experiments show that Cu^0 deposition affects the Faradaic efficiency but this can be counteracted by applying a potential at which Cu^0 will strip from time to time.

C.8 Raman of Cu_2(btmpa) and H_2O_2

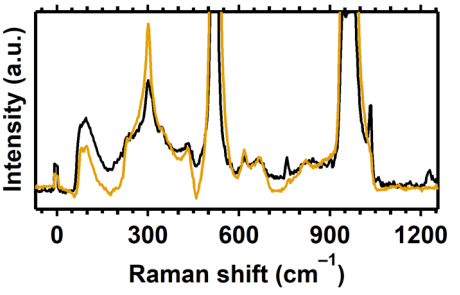

Figure C.12. Raman spectra of a dropcasted solution of 3 mM **Cu_2(btmpa)** (fresh, black) and of a **Cu_2(btmpa)** solution with 22 mM H_2O_2 (orange, 9 days old). The solutions were dropcasted on a silicon wafer.

C.9 References

1. Garribba, E.; Micera, G., *J. Chem. Educ.* **2006,** *83*, 1229.
2. Lee, D.-H.; Murthy, N. N.; Karlin, K. D., *Inorg. Chem.* **1997,** *36*, 5785–5792.
3. Karlin, K. D.; Hayes, J. C.; Juen, S.; Hutchinson, J. P.; Zubieta, J., *Inorg. Chem.* **1982,** *21*, 4106–4108.
4. Langerman, M.; Hetterscheid, D. G. H., *Angew. Chem. Int. Ed.* **2019,** *58*, 12974–12978.
5. Ross, P. N.; Andricacos, P. C., *J. Electroanal. Chem. Interfacial Electrochem.* **1983,** *154*, 205–215.
6. Zhang, Y.; Wilson, G. S., *J. Electroanal. Chem.* **1993,** *345*, 253–271.
7. Hall, S. B.; Khudaish, E. A.; Hart, A. L., *Electrochim. Acta* **1999,** *44*, 4573–4582.
8. Hall, S. B.; Khudaish, E. A.; Hart, A. L., *Electrochim. Acta* **2000,** *45*, 3573–3579.
9. Evans, S. A. G.; Elliott, J. M.; Andrews, L. M.; Bartlett, P. N.; Doyle, P. J.; Denuault, G., *Anal. Chem.* **2002,** *74*, 1322–1326.
10. Katsounaros, I.; Schneider, W. B.; Meier, J. C.; Benedikt, U.; Biedermann, P. U.; Auer, A. A.; Mayrhofer, K. J. J., *Phys. Chem. Chem. Phys.* **2012,** *14*, 7384–7391.
11. Jiang, K.; Back, S.; Akey, A. J.; Xia, C.; Hu, Y.; Liang, W.; Schaak, D.; Stavitski, E.; Nørskov, J. K.; Siahrostami, S.; Wang, H., *Nat. Commun.* **2019,** *10*, 3997.
12. Song, C.; Zhang, J., Electrocatalytic Oxygen Reduction Reaction. In *PEM Fuel Cell Electrocatalysts and Catalyst Layers: Fundamentals and Applications*, Zhang, J., Ed. Springer London: London, 2008; pp 89–134.
13. Hall, S. B.; Khudaish, E. A.; Hart, A. L., *Electrochim. Acta* **1998,** *43*, 579–588.

Appendix D

Supplementary information for Chapter 5:
Mechanistic insight from structure–activity studies in the electrochemical oxygen reduction by substituted tris(2-pyridylmethyl)amine copper complexes

D.1 Electrochemistry of $\mathbf{3}^{NO2}$

The nitro complex $\mathbf{3}^{NO2}$ is, on paper, a very interesting complex since the nitro group has the highest Hammett parameter of all substituents studied here.[2] This high electron withdrawing effect would shift the redox couple significantly and perhaps influence the rate of O_2 reduction. Under argon atmosphere and the same conditions as the other complexes, a sharp reduction starting at 0.4 V was observed with a peak current that was *circa* one order of magnitude higher than expected for a $Cu^{I/II}$ redox couple (Figure D.1). Moreover, no corresponding oxidation was observed. On the other hand, a redox feature at 0.8 V appeared after having scanned below 0.4 V. This feature slowly fades when a narrow potential region was scanned (Figure D.1). The linear relationship between the $E_{1/2}$ and the Hammett parameter that was found for the other complexes (Figure 5.2) would predict a $E_{1/2}$ at circa 0.35 V for $\mathbf{3}^{NO2}$. For this reason, and in combination with the fact that the 0.8 V redox couple is not visible in the first scan, we conclude that the redox feature at 0.8 V does not correspond to the $Cu^{I/II}$ redox couple of the $\mathbf{3}^{NO2}$ complex. It has been reported that 4-nitropyridine can electrochemically be reduced to a hydroxylamine with a total of 6 electrons.[3] Reduction to NH_2 is not expected as the CV's of $\mathbf{3}^{NH2}$ (Figure 5.1) and $\mathbf{3}^{NO2}$ do not match. However, the formed reduced pyridines might be redox active[3] and have some (quasi-)reversible feature that might be linked to the high redox feature at 0.8 V. The redox chemistry of $\mathbf{3}^{NO2}$ is interesting, but disturbs a good assessment of any catalytic properties since the bulk electrolyte will always contain unreacted $\mathbf{3}^{NO2}$.

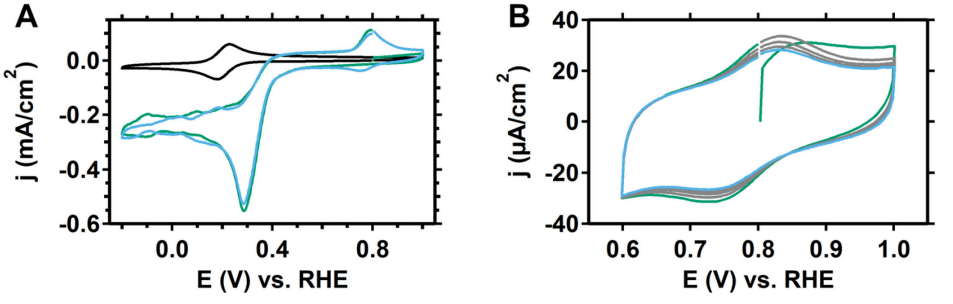

Figure D.1. Cyclic voltammogram under argon atmosphere of $\mathbf{3}^{NO2}$ (green: 1st and blue: 2nd scan) with **1** (black) for comparison (A). B shows 5 scans of the 0.8 V feature of $\mathbf{3}^{NO2}$ after the CV in A was recorded (green first and blue last scan). Different size electrodes were used (0.07 cm^2 for **1** and 0.196 cm^2 for $\mathbf{3}^{NO2}$. The wobbly current response of the first scan in A is due to turbulence created by purging the electrolyte with argon. Data of **1** was adapted from reference 1.

D.2 UV-vis of $\mathbf{2^{Cl}}$, $\mathbf{2^{CF3}}$, $\mathbf{3^{NO2}}$, and $\mathbf{3^{NH2}}$

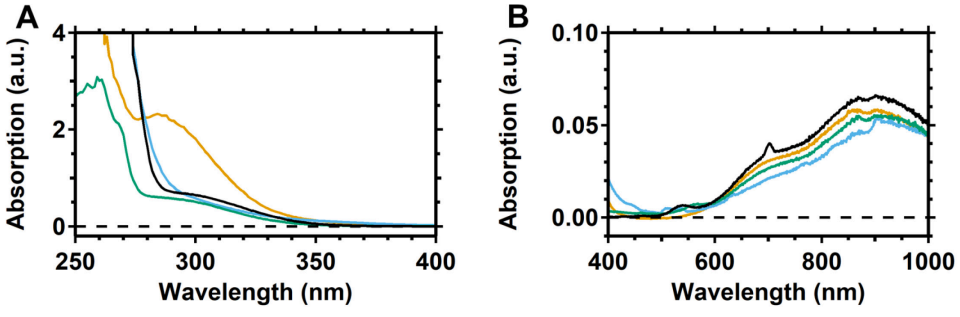

Figure D.2. UV-vis spectra of $\mathbf{3^{NH2}}$ (blue), $\mathbf{3^{NO2}}$ (orange), $\mathbf{2^{Cl}}$ (green), and $\mathbf{2^{CF3}}$ (black) of 0.3 mM solutions of these complexes in 0.1 M phosphate buffer of pH 7.

D.3 Deposition by $\mathbf{3^{NH2}}$

The complex $\mathbf{3^{NH2}}$ could not be purified by crystallization and small remnants of the copper salt $Cu(OTf)_2$ or other impurities may be present in the electrolyte after the *in-situ* formation of the complex. These impurities lead to extra oxidation and reduction peaks in the cyclic voltammograms (Figure D.3) that become visible at low scan rates under argon atmosphere. When the potential was scanned down to −0.2 V, extra oxidative peaks, that grow in current with each consecutive scan, became visible at circa 0.45, 0.55 and 0.70 V (Figure D.3A). In addition, a small reductive peak at 0.4 V was visible after the first scan. In a following scan where the potential was not scanned below 0.0 V, the oxidative peaks disappeared except for the peak at 0.55 V. In addition, the reductive peak at 0.40 V remained. The oxidative peaks are most likely stripping peaks belonging to a Cu^0 deposit that is formed below 0.0 V.

During O_2 and H_2O_2 reduction by $\mathbf{3^{NH2}}$, a broad oxidative feature can be observed (Figure D.3B and D.3C). In addition, after prolonged scanning the O_2 reduction under rotating conditions at potentials as low as −0.6 V revealed two different reductive peaks at 0.4 and 0.5 V. Interestingly, these peaks are accompanied by a spike in ring current as well. On the forward scan to lower potentials, the spike in the ring current is at 0.5 V whereas it can be found at 0.55 V at the backward going scan. This reduction cannot be related to deposit formation since the formed species passes the ring so it must be in solution. It is not known to what species these reductive peaks belong to. However, these peaks only show after prolonged scanning at potentials below −0.6 V, so it is expected that these species do not interfere in the first scan of a CV, especially not in the forward going scan to lower

potentials. The deposition process does take place and affects the CV. However, scanning not lower than 0.0 V will minimize the influence.

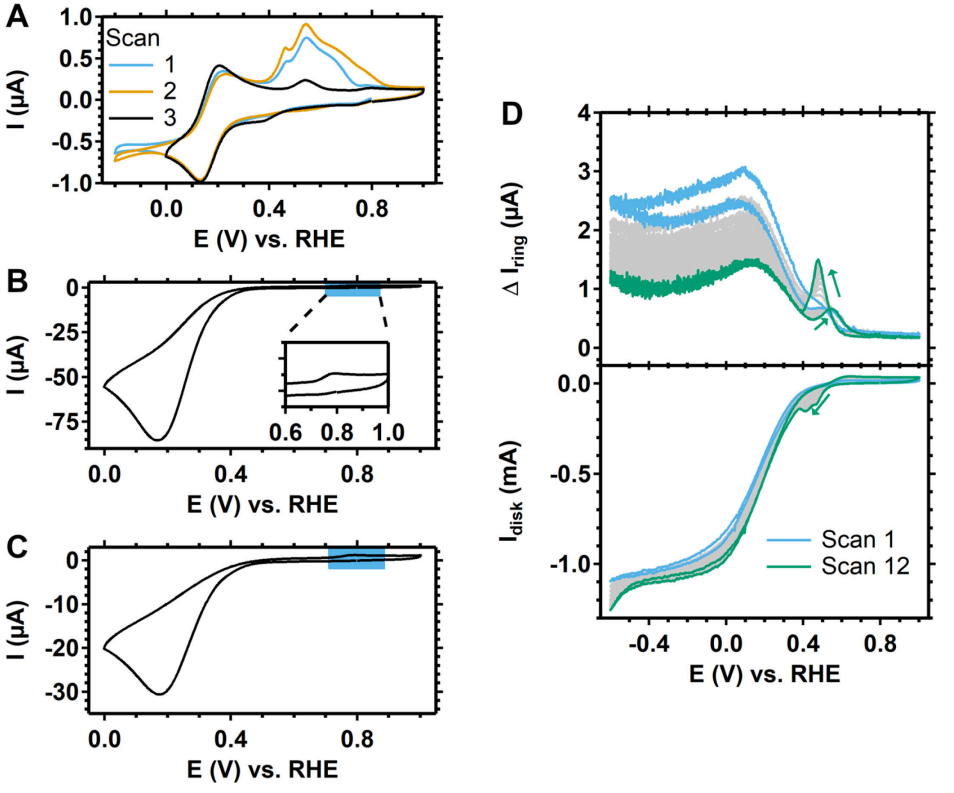

Figure D.3. (A) CVs of $\mathbf{3}^{NH_2}$ under argon atmosphere for which the lower potential of the potential window of the third CV scan was narrowed from −0.2 V to 0.0 V. (B) CV of $\mathbf{3}^{NH_2}$ in the presence of O_2. (C) CV of $\mathbf{3}^{NH_2}$ in the presence of H_2O_2 under argon atmosphere. (D) CVs of $\mathbf{3}^{NH_2}$ with a RRDE setup in O_2 atmosphere with the disk current in the bottom and the ring current in the top panel. The ring potential was 1.2 V throughout the measurement. All CVs were recorded with 0.3 mM catalyst concentration in 0.1 M phosphate buffer of pH 7. Scan rates were 10 (A), 50 (D), and 100 mV/s (B and C).

D.4 Laviron plots of 2^{Cl}, 2^{CF3}, and 3^{NH2}

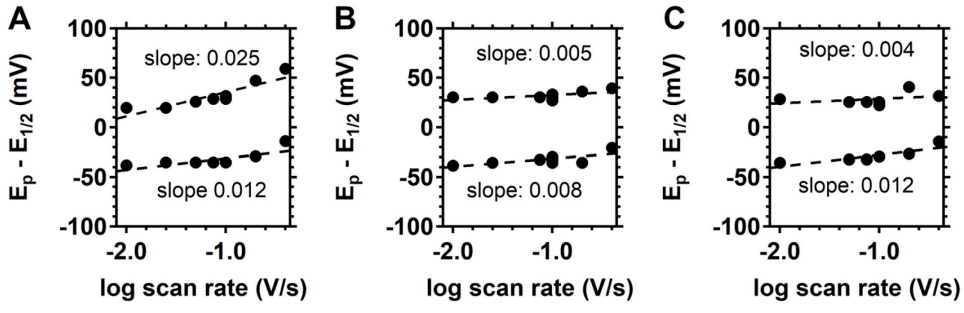

Figure D.4. Laviron plots of the cathodic and anodic peak positions of $\mathbf{2}^{Cl}$ (A), $\mathbf{2}^{CF3}$ (B), $\mathbf{3}^{NH2}$ (C), and the slopes of linear fits (dashed lines).

D.5 Experimental error in O_2 reduction

As with any experiment, there are experimental errors that lead to slight differences between measurements. Under non-rotating conditions, we found that the onset for O_2 reduction by the **1** and $\mathbf{2}^{Cl}$ complexes could differ by *circa* 50 to 75 mV (Figure D.5). This is higher than under rotating conditions (Figure D.6). To investigate whether any onset shifts would be an effect of rotating the electrode, the electrodes were rotated above and below rotation speeds that allow for a diffusion limited current.[4] When rotating too slowly, a peak current is visible. For **1**, varying the rotation speed did not lead to 50 – 75 mV onset potential shifts (Figure D.6) as was the case under non-rotating conditions (Figure D.5). However, the onset is at slightly lower potentials at lower rotation speeds. An explanation for the larger experimental error/onset shift under non-rotating (or very low speed rotating)

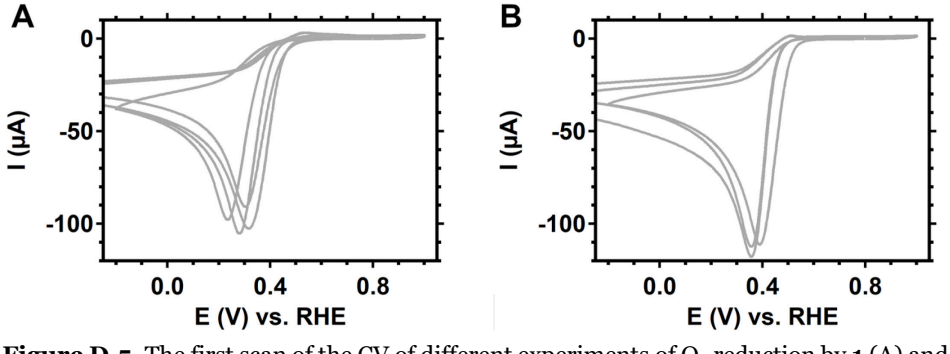

Figure D.5. The first scan of the CV of different experiments of O_2 reduction by **1** (A) and $\mathbf{2}^{Cl}$ (B) with a freshly polished GC electrode (0.07 cm^2) recorded at 100 mV/s in a 0.1 M phosphate buffer of pH 7.

conditions is that electrochemistry is highly dependent on diffusion and thus on turbulence caused by pre-experiment purging of O_2, electrode dipping or other reasons.[4] When rotating fast enough, the effects of turbulence are diminished.

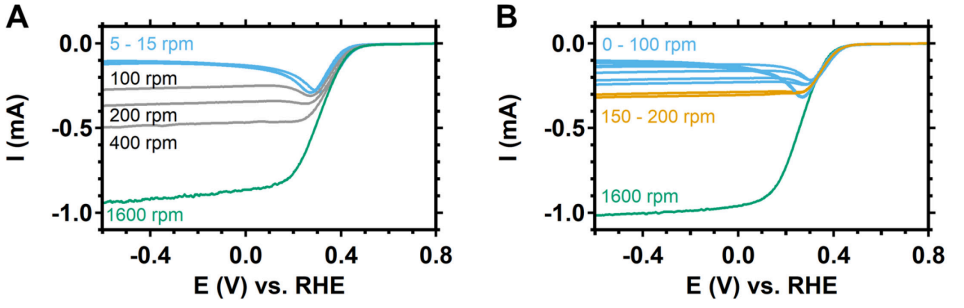

Figure D.6. LSV's of several measurements of O_2 reduction by **1** (A) and $\mathbf{2}^{Cl}$ (B) with a freshly polished GC electrode (0.196cm²) recorded at 50 mV/s in a 0.1 M phosphate buffer of pH 7 at different rotation speeds.

D.6 NMR spectra 6 and 7

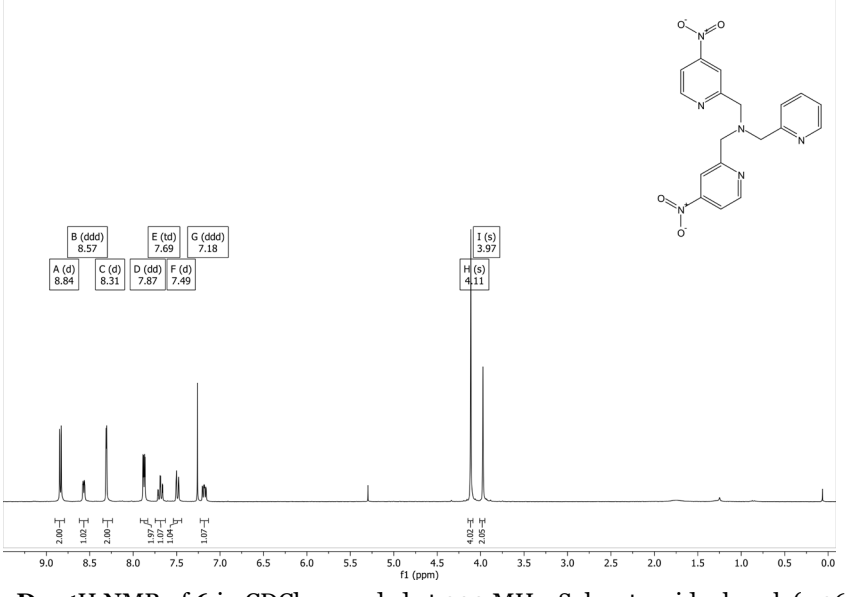

Figure D.7. ^1H NMR of **6** in $CDCl_3$ recorded at 300 MHz. Solvent residual peak (7.26 ppm) and DCM (5.30 ppm) are visible as well.

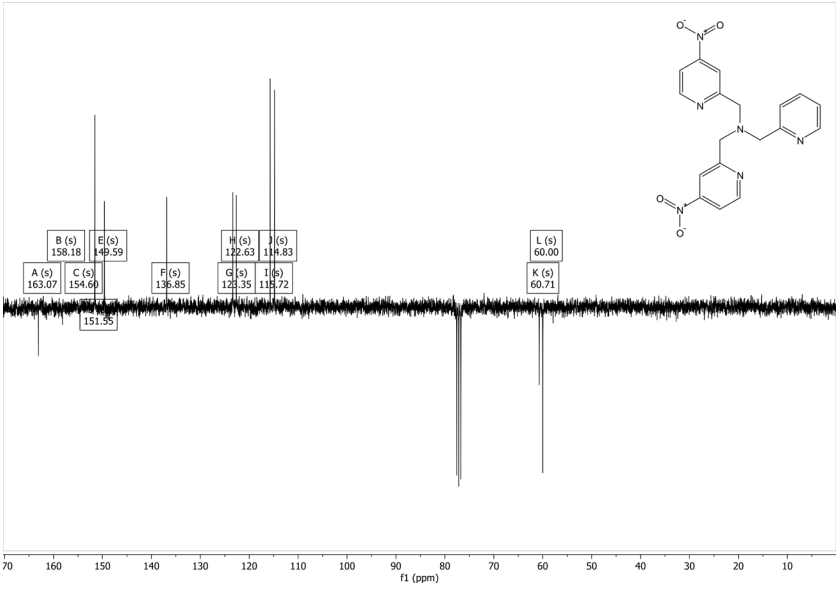

Figure D.8. ^{13}C APT **6** in $CDCl_3$ recorded at 75 MHz. Solvent residual peak is found at 77.16 ppm.

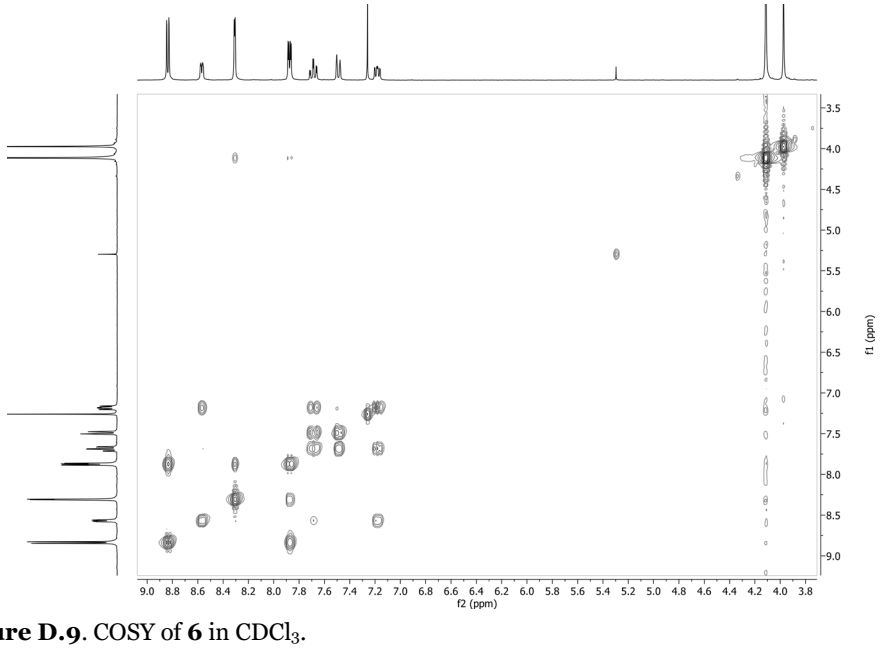

Figure D.9. COSY of **6** in $CDCl_3$.

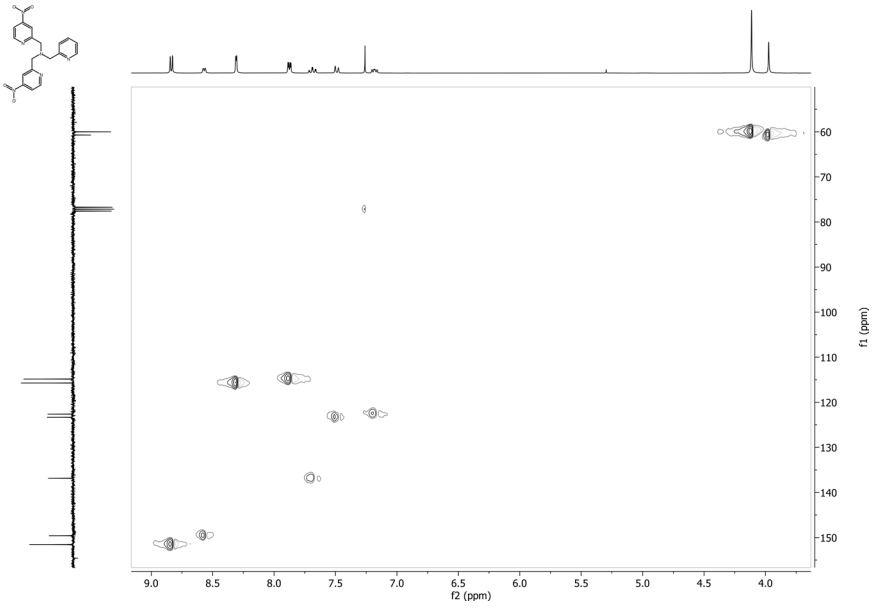

Figure D.10. HSQC of **6** in $CDCl_3$.

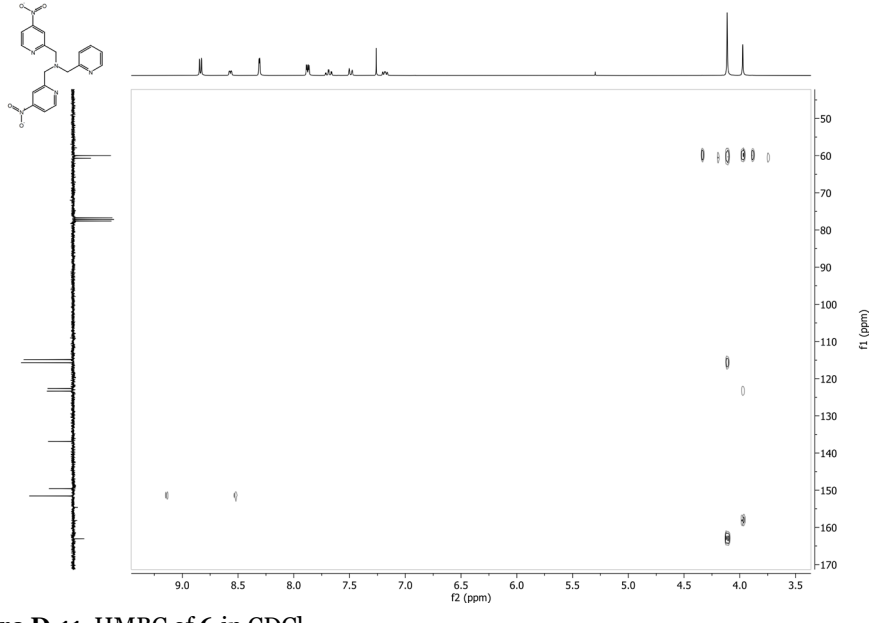

Figure D.11. HMBC of **6** in $CDCl_3$.

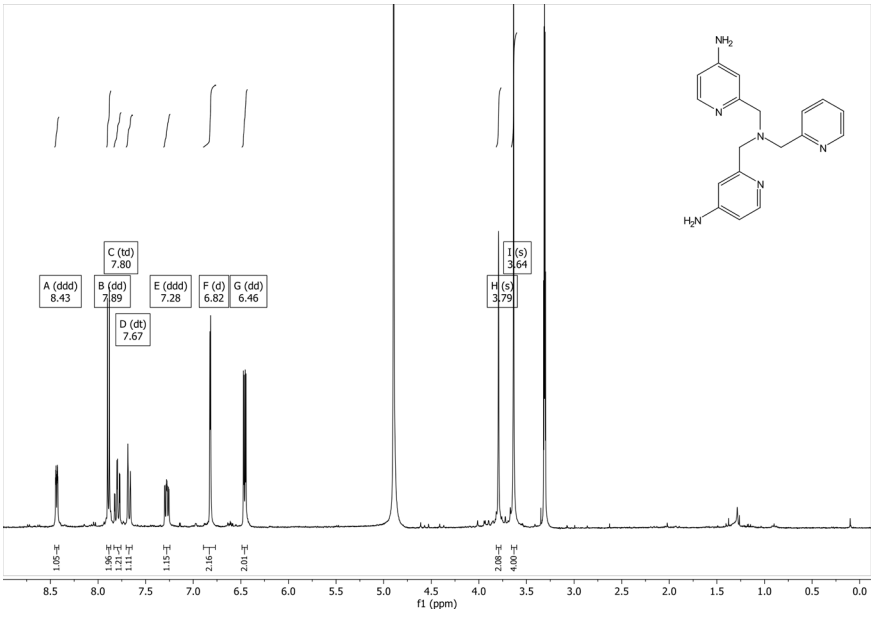

Figure D.12. ^{1}H NMR of **7** MeOD recorded at 300 MHz. Solvent residual peak (3.31 ppm) and H_2O (4.89 ppm) are visible as well.

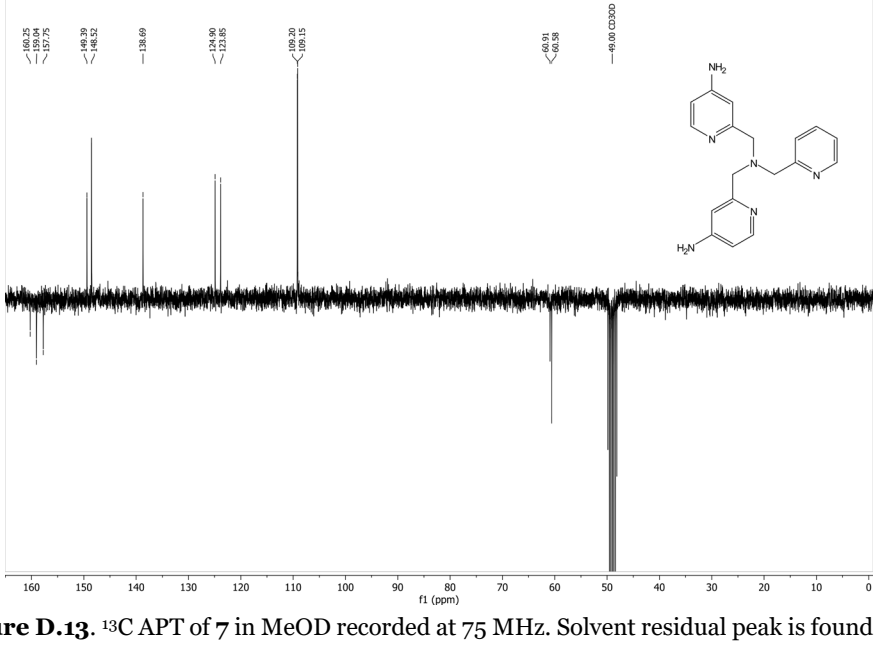

Figure D.13. ^{13}C APT of **7** in MeOD recorded at 75 MHz. Solvent residual peak is found at 49 ppm.

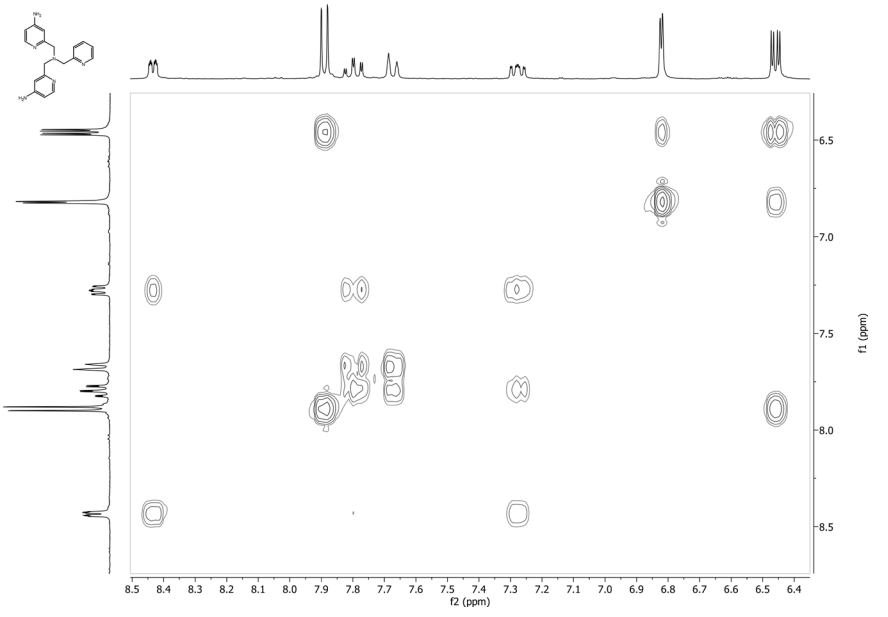

Figure D.14.COSY of **7** in MeOD.

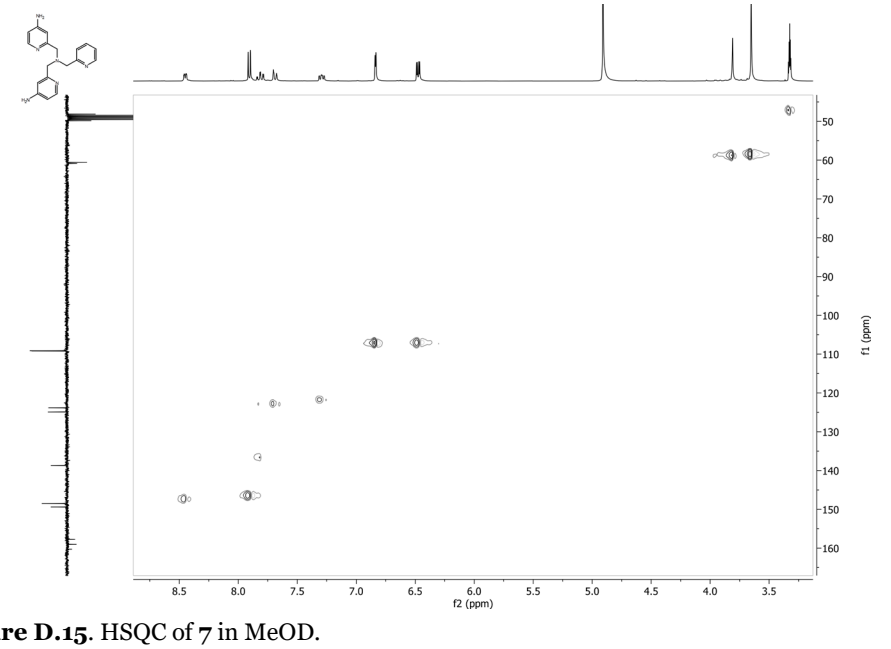

Figure D.15. HSQC of **7** in MeOD.

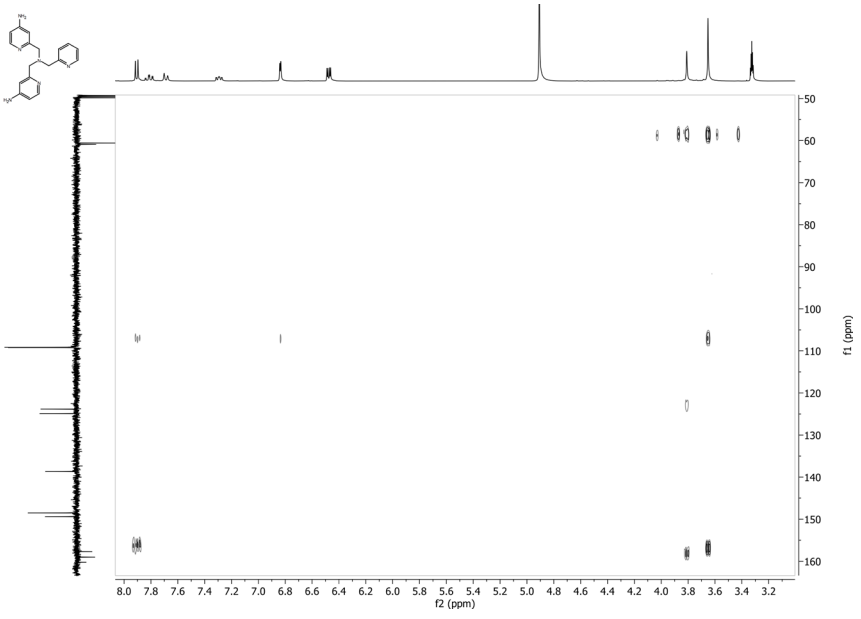

Figure D.16. HMBC of **7** in MeOD.

D.7 References

1. Langerman, M.; Hetterscheid, D. G. H., *Angew. Chem. Int. Ed.* **2019,** *58*, 12974–12978.
2. Hansch, C.; Leo, A.; Taft, R. W., *Chem. Rev.* **1991,** *91*, 165–195.
3. Laviron, E.; Meunier-Prest, R.; Vallat, A.; Roullier, L.; Lacasse, R., *J. Electroanal. Chem.* **1992,** *341*, 227–255.
4. Bard, A. J.; Faulkner, L. R., *Electrochemical Methods: Fundamentals and Applications*. Wiley: New York, 2000.